Molecular probe dynamics and free volume in organic glass-formers and their relationships to structural relaxation: 1-propanol

J Bartoš[1], H Švajdlenková[1], O Šauša[2], M Lukešová[1], D Ehlers[3], M Michl[3], P Lunkenheimer[3] and A Loidl[3]

[1] Department of Structure and physical properties, Polymer Institute of SAS, Dúbravská cesta 9, SK-845 41 Bratislava, Slovakia
[2] Institute of Physics of SAS, Dúbravská cesta 9, SK-845 11 Bratislava, Slovakia
[3] Experimental Physics V, Center for Electronic Correlations and Magnetism, University of Augsburg, D-86135 Augsburg, Germany

Abstract

A joint study of the rotational dynamics and free volume in amorphous 1-propanol (1-PrOH) as a prototypical monohydroxy alcohol by electron spin resonance (ESR) or positron annihilation lifetime spectroscopy (PALS), respectively, is reported. The dynamic parameters of the molecular spin probe 2,2,6,6-tetramethyl-1-piperidinyloxy (TEMPO) and the annihilation ones of the atomic ortho-positronium (o-Ps) probe as a function of temperature are compared. A number of coincidences between various effects in the ESR and PALS responses at the corresponding characteristic ESR and PALS temperatures were found suggesting a common origin of the underlying dynamic processes that were identified using viscosity (VISC) in terms of the two-order parameter (TOP) model and broadband dielectric spectroscopy (BDS) data.

1. Introduction

The structural-dynamic state of organic systems can be basically investigated by two types of experimental techniques. The first group is formed by direct techniques that use the so-called internal probes stemming from the more or less large number of the material's constituents such as static and dynamic density fluctuations in diffraction or scattering techniques [1], or various effective electric dipoles in dielectric spectroscopy [2] etc. Besides these classical techniques, indirect ones based on the addition of very small amounts of an appropriately small probe from the external surroundings of the studied system and monitoring its corresponding behavior are also utilized, however, to a much smaller extent. Recently, combined studies on a series of *amorphous* small molecular [3] and oligo and polymeric [4–7] organic glass-formers of van der Waals and H-bond interaction types by two external probes using electron spin resonance (ESR) and positron annihilation lifetime spectroscopy (PALS) techniques have been reported. The former utilizes one of the smallest stable molecular radicals of the nitroxyl type, the so-called spin probe, 2,2,6,6-tetra-methyl piperidinyl-1-oxy (TEMPO). The temperature dependence of its rotational dynamics was compared with the annihilation behavior investigated by PALS, using the atomic-sized ortho-positronium (o-Ps) probe and, subsequently, with the extracted local free volume parameters of the organics studied. The ESR response of a spin system, namely, the temperature dependence of the spectral parameter,

$2A_{zz'}$, of spin probe TEMPO mobility in a given medium revealed several characteristic ESR temperatures, such as the most pronounced one, T_{50G}, which quantifies *operationally* a main transition of the spin probe from the slow (s) to fast (f) motional regime [8, 9]. Additional ESR temperatures were T^{s}_{Xi} and T^{f}_{Xi}, with $i = 1$ or 2, which reflect subtle changes in the spin probe dynamics within the individual motional regimes [3–7]. Another measure of the spin probe dynamics, i.e. the correlation time, τ_c, of spin probe rotation ranges from 10^{-6} s down to ca. 10^{-9} s in the slow regime and from ca. 10^{-9} s down to 10^{-11} s in the fast one with a typical value at T_{50G} of a few nanoseconds [9]. The PALS response for *the same* amorphous glass-formers, the o-Ps lifetime, τ_3, exhibits several regions of distinct behavior as a function of temperature separated by the characteristic PALS temperatures, namely, T^{G}_{bi}, T^{PALS}_{g}, T^{L}_{b1}, and T^{L}_{b2} [10–13]. Subsequently, the τ_3 values and sometimes also the characteristic PALS temperatures of a series of glass-formers are in very close relationships with various effects in the ESR response, especially above the calorimetric glass temperature, T^{DSC}_{g}. Thus, the averaged mean o-Ps lifetimes at the main characteristic ESR temperature, $\tau_3(T_{50G})$, and at the other one within the fast regime, $\tau_3(T^{f}_{Xi})$, lie in a series of various glass-formers in remarkably narrow ranges of 2.17 ± 0.15 ns [3, 4] or 2.85 ± 0.18 ns [4–7], respectively. According to a standard quantum-mechanical (SQM) model of *o-Ps* annihilation in a *spherical* free volume hole approximation [14], these averaged mean characteristic τ_3 values correspond to the averaged mean free volumes of $V_h(T_{50G}) = 114 \pm 15$ Å^3 [3] or $V_h(T^{f}_{Xi}) = 185 \pm 18$ Å^3, respectively [5–7], the latter one being comparable with the van der Waals volume of the TEMPO molecule [4, 6]. These findings indicate that the afore-mentioned dynamic changes of TEMPO are closely connected with the presence of a certain local free volume that appears to be almost independent of the chemical structure and the related type and extent of vdW- or H-intermolecular bonding [3, 4], the topology of molecules, i.e. small or short versus long) [3, 7] as well as of the physical (glass versus liquid) state [6] of amorphous compounds.

In most organic materials studied so far, the main characteristic ESR temperature is situated above the glass transition temperature with T_{50G} from $T^{DSC}_{g} + 26$ K up to $T^{DSC}_{g} + 93$ K or $(1.10–1.50) \times T^{DSC}_{g}$ [3] with one exception [6], and $T_{50G} - T^{DSC}_{g}$ or T_{50G}/T^{DSC}_{g} strongly depend on the chemical nature of glass-formers. Similarly, the other characteristic ESR temperature T^{fast}_{Xi} $(i = 1,2)$ lie at $T^{DSC}_{g} + 63$ K up to $T^{DSC}_{g} + 138$ K or at $(1.30–1.67) \times T^{DSC}_{g}$ again dependent on the chemical composition of the amorphous compound. At the same time, T_{50G} often coincides quite well with some of the characteristic PALS temperatures such as T^{L}_{b2} and T^{L}_{b1} in the liquid state of small molecule glass-formers or the liquid and elastic state of oligo or polymeric ones, respectively. This suggests common origins of the underlying physical processes independent of the size of the used external probe differing by a factor of ca.10: $R_{o\text{-}Ps} = 0.53$ Å and $R^{W}{}_{TEMPO} = 3.45$ Å. Thus, for fragile vdW- as well as H-bonded small molecule glass-formers such as propylene carbonate (Pc) and meta-toluidine (m-TOL) or the intermediate H-bonded 1,2,3-propanetriol, i.e. glycerol (GL) with quite different fragilities $m_g = 104$ and 84 or 53 [15], respectively, the corresponding T_{50G} values lie close to the so-called plateau effect in the PALS response at T^{L}_{b2} [5, 17–20]. On the other hand, another fragile small molecular glass-former, meta-tricresyl phosphate (m-TCP), with $m_g = 87$ exhibits rather the $T_{50G} \cong T^{L}_{b1}$ relationship [3, 19]. For a series of five homo and hetero-polymers of simple chemical structure without side groups, or at most with very small ones, the corresponding characteristic ESR temperature T_{50G} also compares quite well with the characteristic PALS temperature T^{L}_{b1} [4, 20]. Finally, in some other small molecular glass-formers, T_{50G} lies in between T^{L}_{b1} and T^{L}_{b2} [3, 21].

Next, for some glass-formers the origin of the characteristic PALS temperatures T^{L}_{b2} and T^{L}_{b1} could be identified with the specific motional modes as obtained mainly from broadband dielectric spectroscopy (BDS). Thus, in a series of organic glass-formers studied so far a dramatic bend effect at the so-called plateau temperature T^{L}_{b2} is almost always connected with the approximate identity: $T^{L}_{b2} \cong T_{\alpha}[\tau_{\alpha} = \tau_3(T^{L}_{b2})]$ [16–20], so that the second pronounced effect in the τ_3 versus T dependence is associated with the primary α relaxation. Consequently, on the basis of the closeness of T_{50G} with T^{L}_{b2} as well as of the closeness of the respective *mean* time scales one can also infer that a slow to fast regime transition in the molecular spin probe dynamics may be controlled by the same large-scale structural relaxation process. However, such an identification of the underlying motion responsible for the change in the rotational dynamics of the molecular probe was possible in a few cases only such as the above-mentioned small molecular glass-formers: fragile Pc [3, 17] and m-TOL [3, 18] as well as intermediate GL [3, 16]. On the other hand, as mentioned above, in some small molecular ones, T_{50G} lies in between T^{L}_{b1} and T^{L}_{b2} [3] and the origin of the underlying process remains unclear. Thus, while for the simplest polyalkanol (polyhydroxy alcohol), 1,2,3-propanetriol, i.e. glycerol the approximate identity $T_{50G} \cong T^{L}_{b2}$ is valid, for 1,2-propandiol, i.e. propylene glycol the relation $T^{L}_{b1} < T_{50G} < T^{L}_{b2}$ [3, 21] was found. Therefore, it is of interest to apply both the external probe ESR and PALS techniques, the former in both the dynamic quantities, i.e. $2A_{zz'}$ and τ_c, on a typical representative of the group of monohydroxy alcohols, i.e. 1-propanol, with the *same* number of carbon atoms in the molecule but with one terminal hydroxy group only and to address the role of the extent of the H-bond network on both the ESR and PALS responses and their mutual relationship as well as their relation to internal probe techniques detecting structural relaxation such as viscosity and dielectric relaxation spectroscopy.

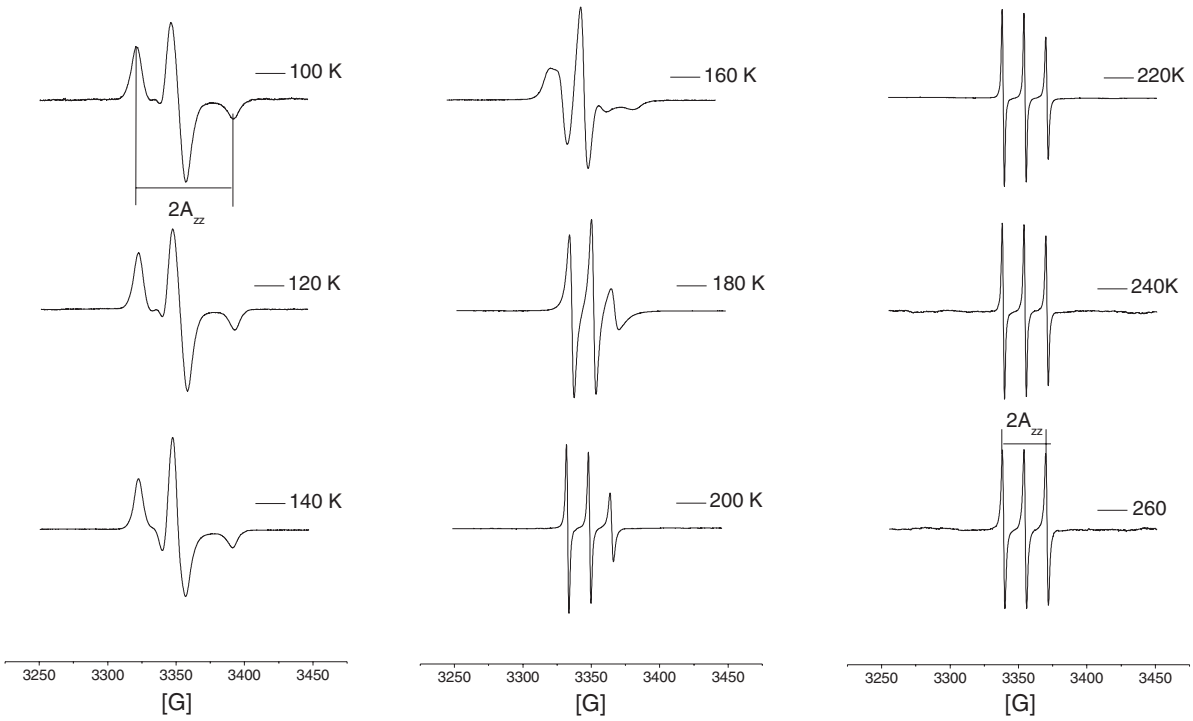

Figure 1. Spectral evolution from broad triplets in the low T region through superimposed triplets in the intermediate T region to narrow triplets at the high-T region of TEMPO in 1-PrOH over a wide T range from 100 K up to 260 K.

2. Experimental

2.1. Materials

1-propanol (1-PrOH) from Sigma-Aldrich, Inc, Germany of 99% purity was used as a medium. The glass temperature was $T_g^{DSC} = 100$ K [22]. As the spin probe, one of the smallest stable free radical of nitroxyl type 2,2,6,6-tetramethyl-1-piperidinyloxy (TEMPO) was utilized at very small concentration of 4×10^{-4} spin mol^{-1} to avoid spectral line distortion of the triplet signal.

2.2. ESR technique

ESR measurements of the spin system 1-PrOH/TEMPO were performed on the X-band Bruker-ER 200 SRL spectrometer operating at 9.4 GHz with a Bruker BVT 100 temperature variation controller unit. The ESR spectra of the slowly cooled doped 1-PrOH/TEMPO system were recorded on heating over a wide temperature range from 100 K up to 270 K with steps of 5 K. To reach thermal equilibrium, the sample was kept at a given temperature for 15 min before the start of three spectra accumulations. The temperature stability was ± 0.5 K. The microwave power and the amplitude of the field modulation were optimized to avoid the signal distortion. Evaluation of the ESR spectra was performed in terms of the spectral parameter of mobility, $2A_{zz'}$, as a function of temperature with a subsequent evaluation of the spectral parameter of the mobility T_{50G} parameter [8] and further characteristic ESR temperatures, $T_{Xi}^{2A_{zz'}}$, in both the slow and fast motional regimes [3–7]. The correlation time, $\tau_c(T)$, as another measure of the spin probe mobility and the corresponding characteristic ESR temperatures such as T_c and further ones, $T_{Xi}^{\tau_c}$, were obtained in two ways: (1) Estimated using semi-empirical expression in the fast regime [9] and (2) evaluated using a Non-linear Least Squares Line (NLSL) simulation program based on the isotropic Brownian model of the spin probe reorientation, which allows the determination of both the time scales, $\tau_{c,}^{s,NLSL}(T)$ and $\tau_{c,}^{f,NLSL}(T)$ and the population fraction $F_s(T)$, $F_f(T)$ of the spin probe TEMPO rotation dynamics in both the slow and fast motion regimes [23].

2.3. PALS technique

The positron annihilation lifetime spectra of 1-PrOH were obtained at the Institute of Physics of SAS, Bratislava by the conventional fast–fast coincidence method using plastic scintillators coupled to Phillips XP 2020 photo-multipliers. The time resolution of prompt spectra was about 320 ps. The radioactive positron ^{22}Na source plus samples assembly was kept under vacuum in a cryogenerator. During the low temperature measurements from 15 K up to 300 K, samples in a holder were fixed at the end of a cold finger of a closed-cycle refrigerator (Leybold) with automatic temperature regulation. The higher temperature study above room temperature (RT) was performed in a chamber without vacuum. The stability of temperature was about 1 K [24]. The positron lifetime spectra were analyzed using the well-known PATFIT-88 software package [25] in terms of a short-term component from *para*-positronium *p*-Ps, τ_1, an intermediate one attributed to 'free' positron, τ_2, and a long-term one, related to free volume: *ortho*-positronium o-Ps, τ_3. The acquisition time per each temperature point was at least 2 h.

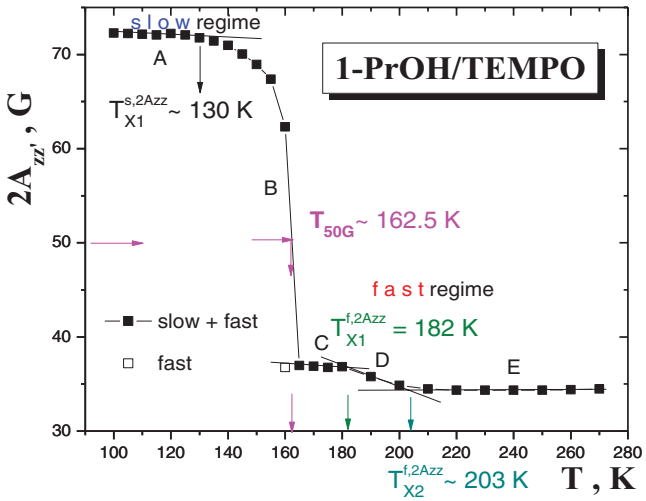

Figure 2. Spectral parameter of mobility of TEMPO in 1-PrOH as a function of temperature. Four characteristic ESR temperatures: $T^{s,2A_{zz'}}_{X1}$, T_{50G}, $T^{f,2A_{zz'}}_{X1}$ and $T^{f,2A_{zz'}}_{X2}$ within the slow and fast motion regimes are marked and discussed in the text. The open square means one case of the ESR spectra just below T_{50G} with the simultaneously distinguished slow and fast components. The error bars do not exceed the point size.

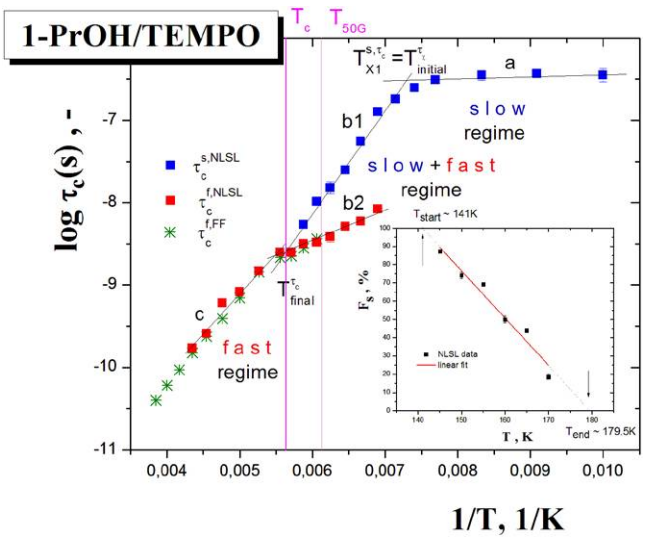

Figure 3. Correlation times, τ_c^{NLSL} and τ_c^{FF}, of TEMPO in 1-PrOH as a function of temperature T. Four regions are described by the Arrhenius equations $\tau(T) = \tau_{\infty,i}.\exp E_i$ /RT with $\tau_{\infty,i}$ in s and E_i in kJ mol^{-1} as follows: (a) Slow regime 100–130 K: $\tau(T) = 2.2 \times 10^{-7}$exp (0.45/RT); (b1) slow regime:140–170 K: $\tau(T) = 2.7 \times 10^{-16}$exp (23.8/RT) (b2) fast regime: 145–170 K: $\tau(T) = 9.3 \times 10^{-12}$exp (8.3/RT), (c) fast regime 180–240 K:τ $(T) = 1.1 \times 10^{-14}$ exp(18.5/RT). The inset displays the population of slow component F_{slow} versus T with a linear fitting giving by extrapolations: $T^{\tau_c}_{start}$ ~ 141 K and $T^{\tau_c}_{end}$ ~ 180 K. The characteristic ESR temperatures are discussed in the text.

3. Results

3.1. ESR data

Figure 1 displays the experimental ESR spectra of the TEMPO probe in 1-PrOH as a function of temperature over a wide temperature range from 100 K up to 270 K with a 20 K step.

The typical course from a broad triplet to a narrow one with increasing temperature with some fine structure in an intermediate region, which will be discussed in detail later, is evident.

The temperature dependence of the first measure of spin probe dynamics, the spectral parameter of mobility of the TEMPO, $2A_{zz'}$, in 1-PrOH is shown in figure 2. Five regions of distinct thermal behavior depicted as A-E can be distinguished. In the lowest T region A, a broad triplet from the slow reorientation of the spin probe is characterized by a linear decrease in the extreme separation of the triplet $2A_{zz'}$ from ca. 72.5 G with an onset of deviation above $T^{s,2A_{zz'}}_{X1} \cong 130\,\mathrm{K} = 1.30\ T^{DSC}_g$. This deviation initiates the slow to fast transition region B with the sharp reduction in $2A_{zz'}$ caused by the averaging of magnetic anisotropy of the molecular probe TEMPO due to some local mobility in its surroundings. The most pronounced effect in the $2A_{zz'}$ versus T plot is *operationally* quantified by the characteristic ESR temperature at $T_{50G} = 163\,\mathrm{K} = 1.63\ T^{DSC}_g$. Finally, three regions C-E of a narrow triplet signal within the fast motion regime are marked by the subsequent characteristic ESR temperatures $T^{f,2A_{zz'}}_{X1} = 182\,\mathrm{K} = 1.82 T_g$ and $T^{f,2A_{zz'}}_{X2} = 203\,\mathrm{K} = 2.03\ T^{DSC}_g$. Note that both the relative characteristic ESR temperatures T_{50G}/T^{DSC}_g and $T^{f,2A_{zz'}}_{X1}/T^{DSC}_g$ for 1-PrOH are higher than those for other glass-formers including H-bonded ones lying in the range of $T_{50G}/T^{DSC}_g \in <1.10;\ 1.50>$ [3] or $T^{f,2A_{zz'}}_{X1}/T^{DSC}_g \in <1.30;1.67>$, respectively.

In figure 3 the correlation times, τ_c^{NLSL}, obtained from the detailed spectral simulations using the NLSL routine over the whole T range from 100 K up to 240 K are presented as a function of 1/T. The inset shows the temperature dependence of the slow component fraction, $F_s(T)$. In contrast to figure 2, *three* basic regions of distinct behavior in the Arrhenius plot, including the slow, the superimposed slow and fast and, finally, the fast regimes (a–c) are evident with some similarities but also some differences with respect to the $2A_{zz'}$ versus T dependence. Thus, in the low-T region the raw broad triplet spectra in the slow motion regime could be reproduced as an one-component spin system, which provides the characteristic ESR temperature $T^{s,\tau_c}_{X1} = 137\,\mathrm{K}$. This region is followed by the ESR spectral region in intermediate T zone b from ca. 145 K up to ca. 170 K characterized by the coexistence of broad (b1) and narrow (b2) triplet signals and finished by high-T region c with the raw narrow triplet modeled as another one-component spectrum again, see figure 4). The intermediate zone b in figure 3 seems to start at around $T^{s,\tau_c}_{X1} = T^{\tau_c}_{initial} \cong 137\,\mathrm{K}$ and to end at $T^{\tau_c}_{final} \cong 178\,\mathrm{K}$, as indicated by the respective crossover points with the low-T slow region a or the fast component region b2, respectively. The extracted population fraction F_s versus T data can be fitted quite well in a linear fashion over the measured points providing the extrapolated boundary temperatures: $T^{F_s}_{initial} \approx 141\,\mathrm{K}$ and $T^{F_s}_{final} \approx 180\,\mathrm{K}$ values corresponding to the limit cases of $F_s = 100\%$ or $F_s = 0\%$, respectively. Strictly speaking, however, for 175 K the raw ESR spectra of TEMPO in 1-PrOH could not be already simulated

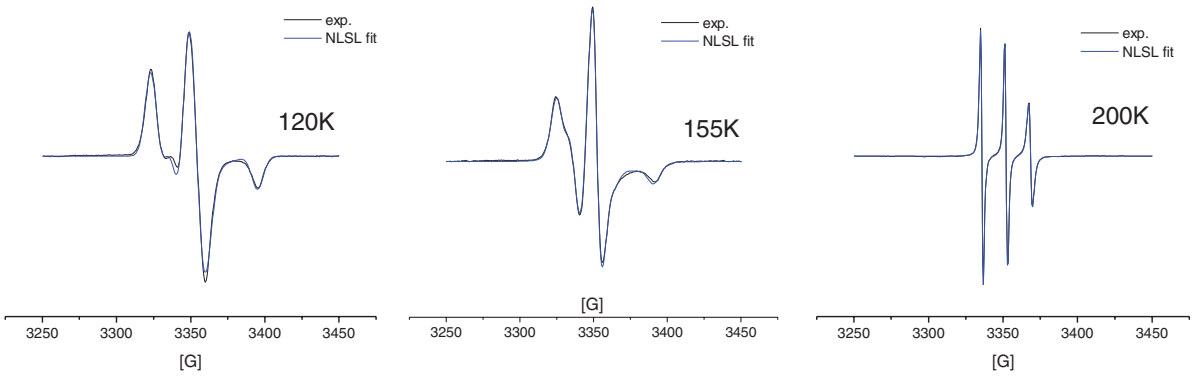

Figure 4. Experimental and simulated ESR spectra of TEMPO in 1-PrOH at the following three representative temperatures 120 K, 155 K, and 200 K in the slow, intermediate, and fast motion regimes.

as a two-component spin system because of the extreme closeness of the respective correlation times and incapability of the NLSL program to distinguish such close values of the correlation times $\tau_c^{s,NLSL}$ and $\tau_c^{f,NLSL}$, so that the true T_{end} seems to lie rather between 170 and 175 K.

The characteristic ESR temperature $T_c = T_{final}^{\tau_c}$ is characterized by the correlation time τ_c^{NLSL} $(T_{final}^{\tau_c}) \cong 2.7 \times 10^{-9}$ s. Thus, while the first crossover temperatures within the slow regime in both the way of analysis agree plausibly with each other, $T_{X1}^{s,\tau_c} \approx T_{X1}^{s,2A_{zz'}} = T_{X1}^{s} = T_{initial}^{\tau_c}$, the operationally defined T_{50G} from $2A_{zz'}$ versus T plot lies *within* the superimposed range b in figure 3, where the ESR spectra can be fitted by a superposition of the slow and fast triplets with two distinct time scales of the spin probe TEMPO. This co-existence of two populations indicates the presence of dynamic heterogeneity in the surroundings of spin probe TEMPO in the intermediate T range of the 1-PrOH. In our case the dynamic heterogeneity as seen by the TEMPO probe can be considered as a reorientation of the spin probe in some 'rigid' or 'mobile' environment of the medium. Finally, at and above the characteristic ESR temperature, $T_{final}^{\tau_c}$, the ESR spectra can be again simulated as the one-component spin system of the spin probes TEMPO in the fast region the τ_c^{NLSL}s. The last characteristic ESR temperature is $T_{X1}^{s,\tau_c} = 183$ K, which results from a cross-section of the correlation time from the fast component in the superposed ESR spectra with the following rapidly decreasing one in high-T fast region c. The activation parameters for all the four distinct regions a–c are given in the caption of figure 3. In addition to simulations, assuming the model of the isotropic rotation of the nitroxide radical [9], the correlation times, τ_c^{FF}, of the spin probe TEMPO in 1-PrOH as a function of temperature over the fast motion regime above $T_{50G} = 163$ K in T range from 170 K up to 270 K as estimated using the semi-empirical Freed–Fraenkel (FF) equation [9] are also plotted in figure 3. Two linear regions indicating different Arrhenius regimes are observed with the following activation parameters: $\tau_{low}(T) = \tau\infty_{,l}\exp[E_l/RT] = 5.4 \times 10^{-12}\exp[8.9\ \text{kJ mol}^{-1}/RT]$ and $\tau_{high}(T) = \tau\infty_{,h}\exp[E_h/RT] = 2.5 \times 10^{-14}\exp[20.9\ \text{kJ mol}^{-1}/RT]$ with crossover at $T_{X1}^{s,\tau_c} = 183$ K in good accordance with $T_{X1}^{f,2A_{zz'}} = 182$ K for $2A_{zz'}$ in figure 2 as well as with $T_{final}^{\tau_c} = 178$ K from figure 3.

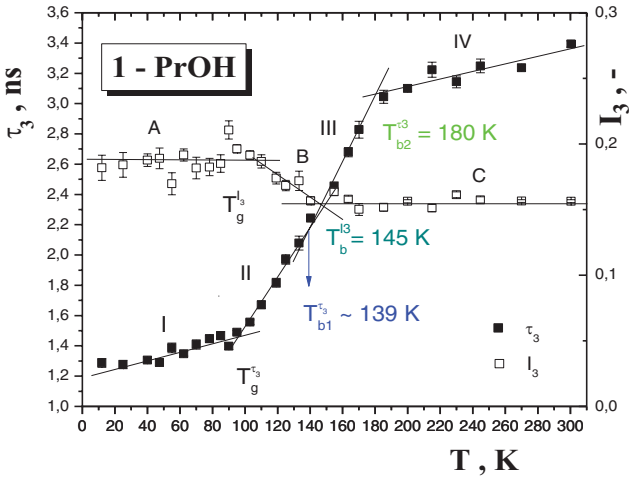

Figure 5. o-Ps lifetime, τ_3, and relative o-Ps intensity, I_3, as a function of temperature T in 1-PrOH with the characteristic PALS temperatures: $T_g^{\tau_3} \cong T_g^{I_3} = T_g^{PALS}$, $T_{b1}^{L,\tau_3} \cong T_{b1}^{L,I_3}$ and T_{b2}^{L,τ_3}.

Note that $T_{X2}^{f} = 205$ K for $2A_{zz'}$ does not have a counterpart in the log τ_c versus $1/T$ plot. Both the correlation times, τ_c^{FF}, and the crossover temperature, $T_{X1}^{f,\tau_c FF}$ as determined from the semi-empirical analysis are in plausible agreement with the corresponding correlation times, τ_c^{NLSL}, and temperature quantity T_{X1}^{f,τ_c} from the spectral simulations.

3.2. PALS data

Figure 5 shows the temperature dependencies of both o-Ps annihilation parameters, namely, the *mean* o-Ps lifetime, τ_3, and the relative *o-Ps* intensity, I_3, as measured in 1-PrOH over an extraordinarily wide T interval from 15 K up to 300 K. The former quantity exhibits roughly a quasi-sigmoidal course, typical for amorphous organic compounds with several distinct regions denoted as I–IV [10–13, 16]. These can be approximated by the following set of linear expressions:
Region I: 47 K–90 K

$$\tau_3 = (2.37 \pm 0.46) \times 10^{-3}\,T + (1.23 \pm 0.03)\ r = 0.935$$

Region II: 103 K–133 K

$$\tau_3 = (1.78 \pm 0.04) \times 10^{-2} T - (0.28 \pm 0.107)\ r = 0.989$$

Region III: 140 K–170 K

$$\tau_3 = (1.98 \pm 0.19) \times 10^{-2} T - (0.55 \pm 0.03)\ r = 0.972$$

Region IV: 200 K–300 K

$$\tau_3 = (2.41 \pm 0.65) \times 10^{-3} T + (2.64 \pm 0.16)\ r = 0.919$$

In the lowest T region I, the o-Ps lifetime,τ_3, and the related free volume, V_h, expand very slightly indicating the almost static structure of the 1-PrOH medium. The first clearly pronounced bend effect in the PALS response is situated at around 100 K and because of its closeness to the calorimetric T_g^{DSC} [22] is marked as $T_g^{\tau_3} = T_g^{PALS}$. On crossing T_g^{PALS}, τ_3 begins to grow relatively rapidly in region II and at $T_{b1}^{L,\tau_3} = 139$ K, the τ_3 versus T plot undergoes a slight change in the slope giving rise to region III. Finally, on a further temperature increase, the second dramatic change in the τ_3 versus T plot is observed, which leads to the lower slope in region IV of the PALS response at the characteristic PALS temperature $T_{b2}^{L,\tau_3} = 180$ K. On the other hand, the relative *o-Ps* intensity, I_3, exhibits three regions A–C with the corresponding characteristic PALS temperatures $T_g^{I_3} \cong T_g^{\tau_3} = T_g^{PALS}$ and $T_{b1}^{L,I_3} \sim$ 140–145 K quite close to T_{b1}^{L,τ_3}. A similar type of dependence was found for glycerol [16]. Analogously to the ESR data, it is of interest to remark that both the relative characteristic PALS temperatures $T_{b1}^{L,\tau_3}/T_g^{PALS} = 1.39$ and $T_{b2}^{L,\tau_3}/T_g^{PALS} = 1.80$ are rather significantly higher than those for the other glass formers studied so far: $T_{b1}^{L,\tau_3}/T_g^{PALS} \in <1.1;1.27>$ or $T_{b2}^{L,\tau_3}/T_g^{PALS} \in <1.26;1.53>$, respectively [3]. This aspect of the problem will be addressed in the discussion section later.

4. Discussion

4.1. Comparisons between the external probe responses

On going from the lowest temperatures of the ESR response, an onset of the decrease in $2A_{zz'}$ with temperature and the first crossover region in the log τ_c^{NLSL}–1/T plot begin in the liquid state above T_g above $T_{X1}^{s} \approx$ 130–137 K, see figures 2 and 3. These changes are followed by the slow to fast transition zone, which is accompanied by the appearance of the superimposed slow and fast spectral region at $T_{initial}^{\tau_c} \approx 141$ K in figure 3 close to the slight effect in the τ_3 versus T plot at $T_{b1}^{L} = 139$ K in figure 5. On heating, the *operationally* defined T_{50G} of the slow to fast transition does not have any counterpart in both the spin correlation time or positron annihilation lifetime. Finally, on further increasing the temperature, the first crossover temperature within the fast region in $2A_{zz'}$ versus T plot at $T_{X1}^{f,\tau_c} \cong T_{X1}^{f,2Azz'}$ after the full disappearance of the slow component as seen in spectral simulations in figure 3 occurs in the vicinity of the second pronounced effect at T_{b2}^{L} in the τ_3 versus T dependence in figure 5. Thus, the superimposed region of the ESR spectra ranges from T_{b1}^{L,τ_3} up to T_{b2}^{L}. In partial summary, some of the crossover effects in both the ESR and PALS responses appear to be closely related and they seem to have the similar origins, which will be discussed in the following subsections.

Next, in this section we address the empirical ESR versus PALS rules found from the $2A_{zz'}$ and τ_3 versus T plots of various glass formers [3]. We find that at $T_{50G} = 162.5$ K both the quantities $\tau_3(T_{50G}) = 2.62$ ns and the corresponding $V_h(T_{50G}) = 160$ Å^3 are significantly higher than expected from the first rule: $\tau_3(T_{50G}) = 2.17 \pm 0.12$ ns and $V_h(T_{50G}) = 114 \pm 15$ Å^3 [3]. In contrast, the o-Ps lifetime at this first characteristic ESR temperature $T_{X1}^{s} = 137$ K achieving the relatively large value of $\tau_3(T_{b1}^{L} = 139\,\text{K}) = 2.1$ ns is rather close to the typical value for the main slow to fast regime transition of a large set of organic glass-formers [3]. On the other hand, at $T_{X1}^{f,2A_{zz'}} \cong T_{X1}^{f,\tau_c} = 182$–183 K, which are very close to $T_{final}^{\tau_c} = 180$ K, the corresponding $\tau_3(T_{final}^{\tau_c}) = 2.7$ ns leads to $V_h = 169$ Å^3 and all the quantities fall into the ranges for the second rule with $\tau_3(T_{X1}^{f,\tau_c A_{zz'}}) = 2.85 \pm 0.18$ ns, i.e. with $V_h(T_{Xi}^{f}) = 185 \pm 18$ Å^3. These findings on the 1-PrOH/TEMPO system suggest that the second rule seems to be more universal than the first one, which is based on the *operational* T_{50G} quantity, at which we still observe the superposed ESR spectra in the 1-PrOH medium, in contrast to $T_{X1}^{f,\tau_c A_{zz'}} \cong T_{X1}^{f,\tau_c} \cong T_{final}$ based on the pure fast ESR ones.

4.2. Comparisons between the external (ESR, PALS) and selected internal (VISC, BDS) probe techniques

In order to interpret the afore-mentioned mutual coincidences between the crossover effects of external probings, the relevant dynamic data from the appropriate internal ones are needed. In figure 6(a) a compilation of all the accessible viscosity data on 1-PrOH from five sources in the literature [26–30] over an extraordinarily wide T range from 103.5 K [30] up to 369 K [26] is presented. Evidently, two regions can be distinguished, namely, a high-T Arrhenius regime and a low-T non-Arrhenius one separated by the characteristic viscosity (VISC) temperature, the so-called Arrhenius temperature: $T_A^{\eta} = 176$ K, as often observed for many glass-formers also by other techniques [31–35]. Note that the melting temperature of the crystalline 1-PrOH, which is prepared under special thermal conditions, is $T_m = 149$ K [22], i.e. T_A lies somewhat above T_m in the normal liquid state of 1-PrOH in accordance with many other organic glass-formers [31].

In the literature, several phenomenological models exist that try to account for the dynamics of glass-forming organic compounds over a wide temperature range [37–41]. These approaches based on the extended free volume (EFV) model [36], the coupling model (CM) [37] and the frustrated-limited domains (FLD) model [38] have been proposed to interpret the physical nature of these characteristic dynamic temperatures. Recently, a joint diffraction and computer modeling work indicated the presence of cluster-like heterogeneities in a few amorphous glass formers [39]. These structural findings could be plausibly explained in terms of *solid* and *liquid*-like domains of the hetero-phase fluctuation (HPF) [40] or the two-order parameter (TOP) model [41]. In this

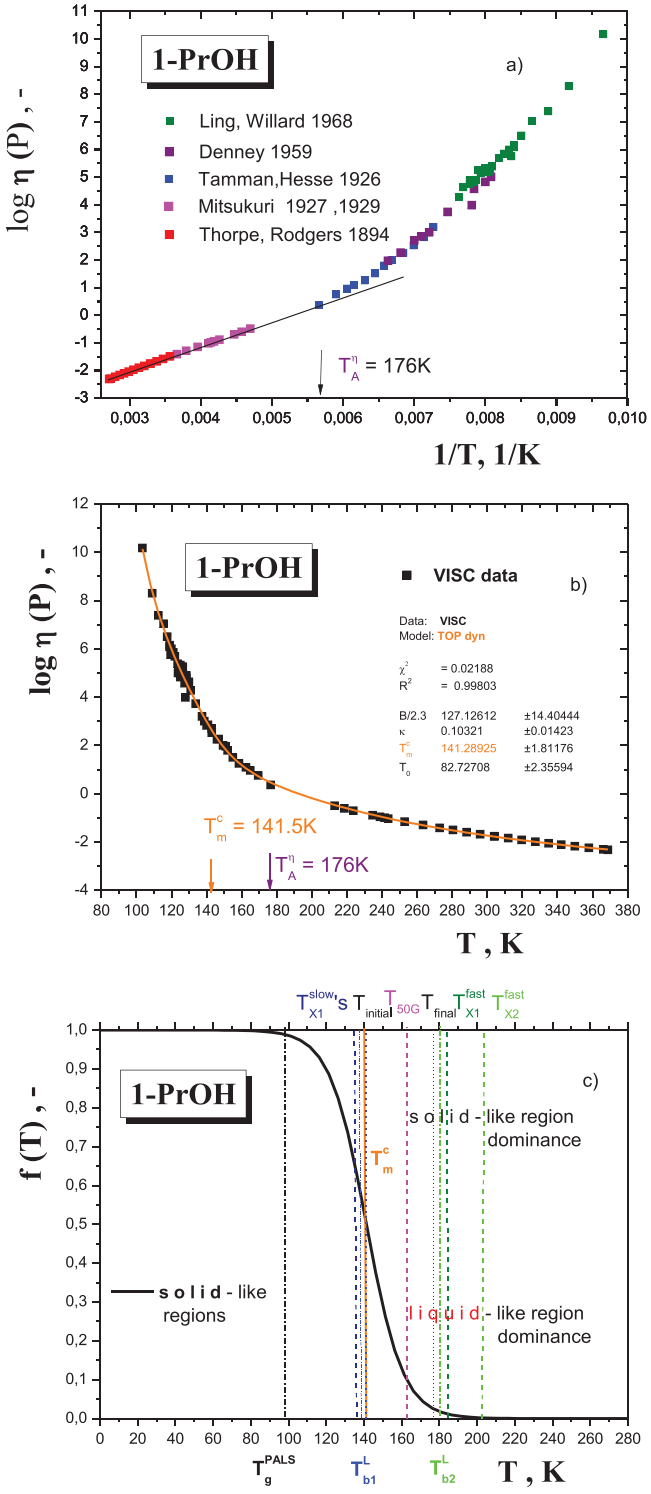

Figure 6 (a–c). Compilation of the viscosity data with a manifestation of the two distinct dynamic regimes at $T_A = 176$ K (a) together with their phenomenological analysis in terms of the TOP model with the pre-exponential factor $\eta\infty = 1.5 \times 10^{-5}$ P and the activation energy $E_{n_\infty} = 17.8$ kJ mol^{-1} (b) and the probability of *solid*-like domains, $f(T)$, as calculated from the fitting parameters of the TOP model (c). The characteristic ESR temperatures: T_{X1}^s's, $T_{initial}^{\tau_c}$, T_{50G}, $T_{final}^{\tau_c}$, T_{X1}^f and T_{X2}^f and the characteristic PALS temperatures T_g^{PALS}, T_{b1}^L and T_{b2}^L as well as the characteristic TOP temperature T_m^c depicted as vertical lines are marked and discussed in detail in the text.

paper it is demonstrated that the log η versus T data over an extraordinarily wide T range in figure 6(b) can be satisfactorily described in terms of the TOP model of supercooled and normal liquid dynamics [41]:

$$\eta(T) = \eta_\infty \exp[E_\eta^*/RT] \exp[Bf(T)/(T - T_0)] \qquad (1)$$

where $\eta(T)$ is the viscosity, η_∞ is the pre–exponent factor, E_η^* is the activation energy above $T_m^* \approx T_A$, T_0 is the divergence temperature, B is the coefficient, and $f(T)$ is a probability function for *solid*-like domains. The latter quantity is defined as

$$f(T) = 1/\{\exp[\kappa(T - T_m^c)] + 1\} \qquad (2)$$

where κ describes the sharpness of the probability function between *solid*-like and *liquid*-like domains and T_m^c is the characteristic TOP temperature. This is the critical temperature where the free energy of a crystallizing liquid is equal to that of the crystal $\Delta G_{lq} = \Delta G_{cr}$ or, in the general case of non-crystallizing glass-formers, the free energy of a non-crystallizing liquid is equal to that of a solid:$\Delta G_{lq} = \Delta G_{sol}$.

The physical picture of glass-forming liquids covering the glassy, the supercooled liquid state, as well as the normal liquid state of 1-PrOH in terms of the temperature dependence of the *solid*-like domain probability $f(T)$ following from this fitting of the viscosity is depicted in figure 6(c). As will be shown, this specific model of glass-forming liquids is useful to explain the ESR and PALS findings.

Thus, the characteristic ESR and PALS temperatures $T_{X1}^s = 130$–137 K $\cong T_{b1}^{L,\tau_3} = 139$ K are quite close to the characteristic TOP one $T_m^c = 141 \pm 2$ K indicating that an onset of the slow to fast transition of the spin probe TEMPO, which approximately coincides with the slightly enhanced expansion of the free volume in the PALS one at T_{b1}^{L,τ_3} may be associated with a crossover in the dominance between the *solid*-like and *liquid*-like domains within the non-Arrhenius regime of supercooled liquid and the related 'softening' of the 1-PrOH matrix.

Next, almost immediately after crossing T_{X1}^s, the ESR spectra of TEMPO in 1-PrOH could be reproduced as a superposition of the slow one with the relatively sharply decreasing correlation time, $\tau_{c,s}^{NLSL}$, and of the fast spectral component with a slightly changing $\tau_{c,f}^{NLSL}$ at ca. $T_{initial} \approx 141$ K, which indicates the co-existence of slow and fast moving probes persisting effectively up to 170–175 K. It is of interest that *also* this initial temperature of this appearance of the fast moving spin probes on the ns-scale with an activation energy of a few kcal/mol is very close to the characteristic TOP temperature, T_m^c, where the *liquid*-like domains begin to dominate over the *solid*-like ones. On the opposite side, the disappearance of the coexistence of slow and fast moving spin probes TEMPO is close to the Arrhenius temperature T_A, where the *solid*-like zones almost completely disappear. This ESR finding indicates that the spin probe TEMPO 'feels' two different dynamic surroundings in the medium and that the dynamic heterogeneity of 1-PrOH as monitored by the external molecular TEMPO probe does exist in between T_m^c and T_A, i.e. even in the 'normal' liquid state above T_m of crystalline 1-PrOH up to

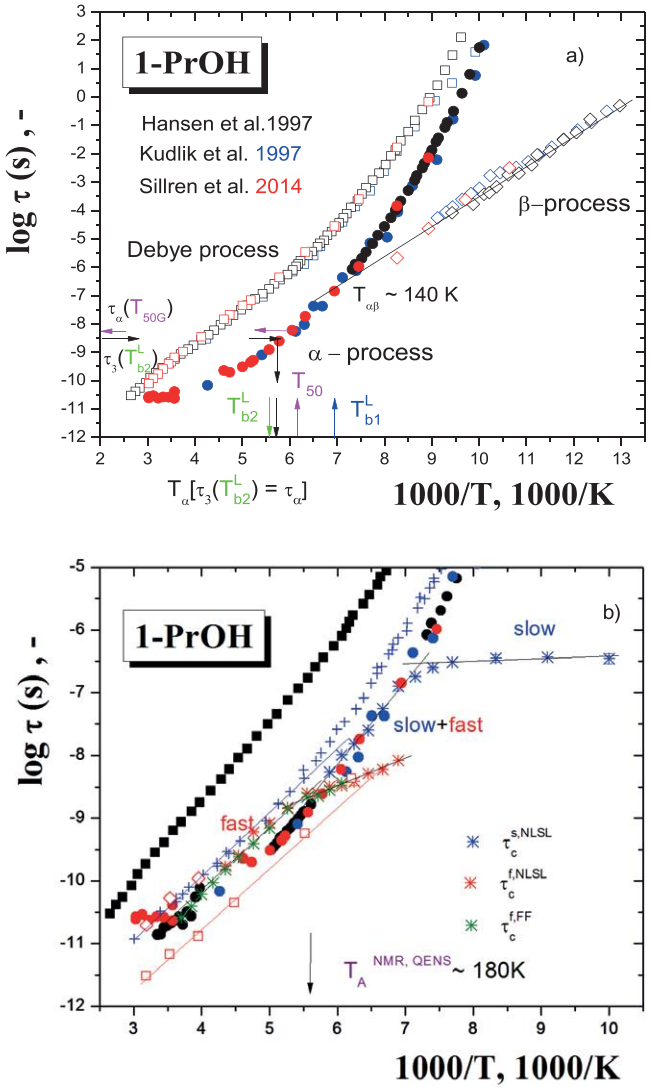

Figure 7. (a) Compilation of the dielectric relaxation times indicating the presence of three distinct relaxation processes: Debye relaxation, primary α relaxation, and secondary β relaxation [42–44]. The relevant characteristic BDS ($T_{\alpha\beta}$, T_α), PALS ($T^{\rm L}_{\rm b1}$, $T^{\rm L}_{\rm b2}$) and ESR ($T_{\rm 50G}$) are indicated in figure b. Details of the high T and high f part of the relaxation map also containing the relaxation times from other techniques: NMR (crosses) [45] and QENS for scattering vector $Q = 1.4$ 1/Å corresponding to the main peak (empty squares) and for $Q = 0.7$ 1/Å belonging to the pre-peak of the structure factor (empty diamonds) from 44. The correlation times, $\tau_{\rm c}$, of the TEMPO probe from the spectral simulations are shown as blue and red stars and those from the semi-empirical rotational model are included as green stars.

the dominance of the Arrhenius regime in the viscosity, where only the fast moving spin probes exist. These findings seem to suggest some association between slowly moving probes and *solid*-like domains of the medium connected according to the TOP model with the rearrangement of the *solid*-like domains postulated to be the structural relaxation process [41] both exhibiting a decreasing trend with increasing temperature. This hypothesis about the origin of the slow component implies a coupling of the times scales of the spin probe dynamics with the structural relaxation and this issue will be discussed in the next paragraph. At the same time, the range of dynamic heterogeneity detected by ESR overlaps with the higher-T liquid range in the PALS response from $T^{\rm L}_{\rm b1}$ up to $T^{\rm L}_{\rm b2}$. Note that according to the TOP model, the *solid*-like domains persist over the melting temperature of the *crystalline* form of 1-PrOH, i.e. into the normal liquid, so that this picture appears to be consistent with the ESR finding of the dynamic heterogeneity of the 1-PrOH sample.

4.3. BDS data

To identify in more detail the motional mode(s) responsible for the observed effects in the ESR and PALS response, a compilation of three dielectric relaxation dataset sources [42–44] over an extraordinary T range from 77 K up to 377 K is of relevance, see figure 7(a). The following three basic dielectric relaxation processes exist: The slow Debye process, primary α relaxation, and fast secondary β process with the non-Arrhenius character for the former two and with the Arrhenius one for the latter. These can be confronted with the spin probe dynamics at two levels: (i) characteristic time scales and (ii) characteristic temperature(s).

Figure 7(b) displays the relevant time scales of ESR from figure 3 together with those from BDS [42–44], NMR [45] and QENS [42]. As seen, the TEMPO mobility in the slow regime a is fully decoupled, i.e. is more rapid with a much lower activation energy than both the mean primary α relaxation time as well as from the mean secondary β process. On increasing the temperature, the time scale of the spin probe TEMPO approaches that of the primary α relaxation, and at around 140–145 K the slow component from the superimposed ESR spectra, $\tau_{\rm c}^{\rm s,NLSL}$, becomes merged with the *mean* relaxation time of the structural relaxation,τ_α, and both lines continue together up to 170–175 K. This indicates that the structural α process governs the TEMPO reorientation in between ca. 140 and 170–175 K. It is of interest that around this merging region the fast component in the superimposed ESR spectra just begins to occur. As seen in figure 8 the time scale of the fast component of the spin probe TEMPO transformed into the equivalent frequency, $f_{\rm c}^{\rm eq}(T) = 1/(2\pi\tau_{\rm c}(T))$, reaches the high-frequency tail of the primary α peak in the decomposed BDS spectra for two very close temperatures: 134 K and 144 K. A similar relationship occurs for the slight bend effect at $T^{\rm L}_{\rm b1} = 139$ K in the PALS response, as expressed by means of the equivalent frequency $f^{\rm eq}_{\rm 3,b1}(T) = 1/(2\pi\tau_3(T))$. This is another indication that the dynamic heterogeneity of the spin probe TEMPO in 1-PrOH is related to the primary α process.

On further heating, the TEMPO correlation time leaves the trace of $\tau(T)$ of the primary α relaxation deduced from BDS, but both dependencies follow a parallel course, except in the very high-T region. As discussed in 44, this rather atypical course of the dielectric relaxation time is due to the mutual influence of the very close Debye process, which causes significant uncertainties in spectral analysis. On the other hand, further relaxation times from other dynamic techniques, namely, from NMR [45] and QENS [42] provide the expected linear Arrhenius behavior above $T_{\rm A} = 175$ K–180 K in full consistency with the viscosity data in figure 6(a) [26–30].

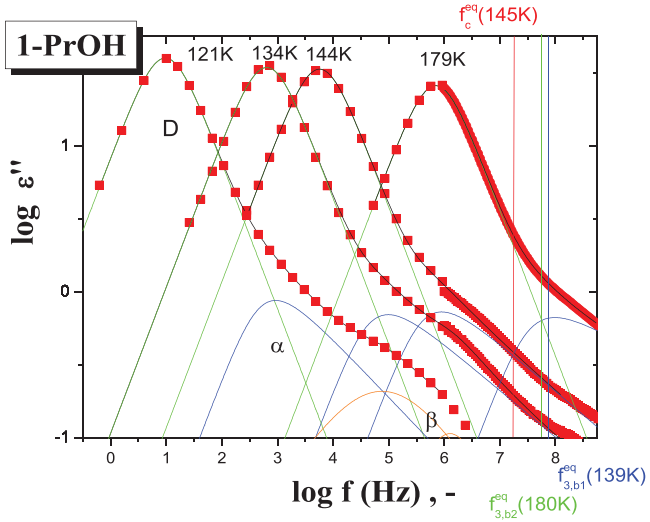

Figure 8. The BDS spectra of 1-PrOH at four temperatures decomposed into three components, i.e. the Debye process (green), the primary α process (blue), and secondary β relaxation (orange) at 121 K and 134 K or into two, i.e. Debye (green) and primary α process (blue) at 144 K and 179 K. The equivalent ESR and PALS frequencies corresponding to the respective effects in the ESR and PALS responses at close temperatures 139 K and 145 K fall into the high-frequency tail of the primary α peak. The equivalent PALS frequencies corresponding to the onset of lower slope in the PALS responses at 179 K lie close to the peak maximum of the primary α process.

These findings indicate that the structural relaxation process influences the TEMPO reorientation above 185 K.

Next, the corresponding analyses of the broadband dielectric spectroscopy (BDS) relaxation time data give several characteristic BDS temperatures that are also in a remarkable relationship to both the characteristic ESR and PALS temperatures T^{s}_{X1} or T^{L}_{b1}, respectively. Thus, the first obtained relaxation times about all three processes from Hansen *et al* [42] using a derivative Stickel's type analysis [46] provided the characteristic BDS temperature $T^{ST}_{B} = 138$ K [42]. As mentioned in [42], this value agreed with another characteristic BDS temperature, the extrapolated $\alpha\beta$ merging temperature $T_{\alpha\beta} = 138$ K. This simple extrapolation appears to be supported by the very recent BDS study [40]. All three datasets of the secondary β relaxation times including the ones within the liquid state from [42–44] can be accounted for by the Arrhenius equation: $\tau_\beta = \tau_{\beta\infty}\exp[E_\beta/RT] = 1.42 \times 10^{-14}\exp[10.4\ \text{kJ mol}^{-1}/RT]$. A subsequent extrapolation towards the primary α relaxation times gives $T_{\alpha\beta} = 140$ K, in accordance with the original value on the limited glassy dataset only: $T_{\alpha\beta} = 138$ K [42, 47] and also with the other characteristic BDS temperature relating to the primary process, T^{ST}_{B}, as well as with the characteristic ESR and PALS temperatures. Moreover, all these external (T^{s}_{X1}, T^{L}_{b1}) as well as internal (T^{ST}_{B}, $T_{\alpha\beta}$) probe findings appear to be consistent with the TOP model with the characteristic TOP temperature, above which the *liquid*-like domains begin to dominate over the *solid*-like ones formed by more or less dense clustered molecules. In particular, the disappearance of the secondary β process above $T_{\alpha\beta} \cong T^{c}_{m}$ appears to be strongly related to a change in the character of the primary α process at T^{ST}_{B}, and both dynamic phenomena seem to be connected with the loss of the dominance of the *solid*-like domains in favor of the *liquid*-like ones.

In the fast motional regime, two changes in the $2A_{zz'}$ versus T dependence (figure 2) at the characteristic ESR temperatures $T^{f,2A_{zz'}}_{X1} = 182$ K and $T^{f,A_{zz'}}_{X2} = 203$ K and one change in the log τ_c versus $1/T$ plot (figure 3) at the characteristic ESR temperatures $T^{f,\tau_c}_{X1} = 183$ K indicate the further averaging of the magnetic anisotropy of the spin probe TEMPO dynamics. The T^{f}_{X1} values are consistent with the characteristic PALS temperature of the onset of the lower slope effect in the PALS response at $T^{L}_{b2} \cong 180$ K. Further, by a comparison of the corresponding o-Ps lifetime with the time scale of the primary α process we find a plausible accord with the so-called equivalent α temperature T^{PALS}_{α} [$\tau_3(T^{L}_{b2}) = \tau_\alpha = 3.1$ ns] = 172 K, which indicates the mutual connection of an onset of the bend effect in the PALS response and the structural dynamics of 1-PrOH. As mentioned above the relative characteristic PALS temperature T^{L}_{b2}/T_g is significantly higher compared to those for the other glass-formers studied so far [3]. This is true even for highly H-bonded systems such as polyalcohols with the same number of carbon atoms in the molecule, i.e. 1,2-propanediol (propylene glycol) and 1,2,3-propanetriol (glycerol) with $T^{L}_{b2}/T_g = 1.53$ [3]. These findings are consistent with an essentially smaller fragility of 1-PrOH $m_g = 40$ [48] in comparison with similar fragilities of both the related polyalcohols: $m_g = 52$ or 53, respectively [15].

In the context of the PALS and BDS data, it is important to mention that the finding $T^{L}_{b2} \cong 180$ K versus T^{PALS}_{α} is not inconsistent with an alternative interpretation of the plateau effect in the PALS response based on the so-called bubble effect of the quantum-mechanical o-Ps particle in a low viscosity medium [49]. Note that while the plateau effect within this scenario is an artefact of the PALS techniques due to strong interaction between the quantum-mechanical o-Ps particle and the low viscosity medium, in the case of ESR this is not the case and the molecular probe reflects the *true* change in the structure-dynamic state of the medium. Evidently, this is connected with the classical character of the used molecular probe versus the quantum-mechanical one of the used atomic probe. Both the dramatic changes in the TEMPO dynamics at T^{f}_{X2} as well as the *o-Ps* annihilation at T^{L}_{b2} appear to be consistent with the output of the TOP model, i.e. a low level of the fraction of the *solid*-like domains close to T_A, see figure 6(c).

Finally, the $T^{f}_{X1} = T^{L}_{b2} \cong T_\alpha$ relationships between all three phenomena suggest that the primary α process also takes part in the spin probe TEMPO reorientation in the fast motion regime. This is supported by the closeness of the equivalent frequency $f^{eq}_{3}(T^{L}_{b2})$ to the maximum frequency of the primary α process from the decomposed BDS spectra at 179 K in figure 8. In addition, all these three characteristic ESR, PALS, and BDS temperatures are close to the characteristic VISC temperature, $T_A = 176$ K, where the structural relaxation dynamics is closely related to the viscosity changes from the non-Arrhenius to the Arrhenius regime. Thus, on the basis

of the approximate identity of the correlation times in the slow regime of the superimposed region *b* with the *mean* relaxation times from BDS, we can conclude that the primary α process governs the spin probe TEMPO reorientation in intermediate T region above $T_{X1}^{s} = T_{B}^{ST} = T_{\alpha\beta}$ up to ca. 170 K–175 K. Further, on the basis of the closeness and parallelism of the correlation time in the fast motion regime *c* with the *mean* relaxation times from NMR and BDS (except of very high Ts) as well as the similarity of the ESR activation energies together with those from NMR and QENS we can infer that the primary α process closely influences the spin probe TEMPO reorientation in the high T region c above $T_{X1}^{f} = T_{A}$.

5. Conclusion

We have presented a combined ESR and PALS study of the rotational dynamics and free volume in amorphous 1-propanol (1-PrOH) as a prototypical monohydroxy alcohol. The dynamics of the molecular spin probe TEMPO, characterized by the spectral parameter of mobility and the correlation time, and the dynamics revealed by the annihilation of atomic o-Ps probe in terms of the o-Ps lifetime and the related free volume as a function of temperature, were compared and numerous coincidences between various effects in the ESR and PALS responses at the corresponding characteristic ESR and PALS temperatures were found. These coincidences suggest a common origin of the underlying motional processes that were discussed within the TOP model in terms of *solid*-like and *liquid*-like domains using the viscosity data. Subsequently, and consistent with this model, the underlying dynamic process is identified by means of broadband dielectric spectroscopy data. In the low-T region within the pure slow motion regime a strong decoupling between the spin probe dynamics and all three relaxation processes in 1-PrOH exists. On the other hand, in the intermediate T range the TEMPO reorientation is dynamically heterogeneous with the reorientation in the slow regime being closely controlled by the *mean* primary α process, while the fast component is related to the high-frequency tail of this relaxation. Finally, in the highest T interval the dynamics of spin probe TEMPO within the pure fast regime is continuously influenced by structural relaxation.

Acknowledgments

This work was supported by the Germany-Slovak DAAD-SAS 2015 grant and by the VEGA Agency, Slovak Academy of Sciences via project 2/0017/12 (J B). The first author thanks Prof D E Budil for providing us with his simulation program.

References

[1] Lovesay S W *et al* 1987 *Theory of Neutron Scattering from Condensed Matter* (Oxford: Clarendon)
Beé M 1988 *Quasi-Elastic Neutron Scattering* (Bristol: Adam Hilger)
[2] Kremer F and Schönhals A 2003 *Broadband Dielectric Spectroscopy* (Berlin: Springer)
Lunkenheimer P, Schneider U, Brand R and Loidl A 2000 *Contemp. Phys.* **41** 15
[3] Švajdlenková H, Šauša O, Iskrová-Miklošovičová M, Majerník V, Krištiak J and Bartoš J 2012 *Chem. Phys. Lett.* **539–540** 39
[4] Švajdlenková H, Iskrová M, Šauša O, Dlubek G, Krištiak J and Bartoš J 2001 *Macromol. Symp.* **305** 108
[5] Švajdlenková H and Bartoš J 2009 *J. Polym. Sci.* B **47** 1058
[6] Bartoš J, Švajdlenková H, Yu Y, Dlubek G and Krause-Rehberg R 2013 *Chem. Phys. Lett.* **584** 88
[7] Bartoš J, Švajdlenková H, Lukešová M, Yu Y and Krause-Rehberg R 2014 *Chem. Phys. Lett.* **602** 28
[8] Rabold G P 1969 *J. Polym. Sci.* A **17** 121
[9] Veksli Z, Andreis B and Rakvin B 2000 *Prog. Polym. Sci.* **25** 949
Cameron G G 1989 *Comprehensive Polymer Science* vol 1 ed C Booth and C Price (Oxford: Pergamon) p 517
Törmälä P 1979 *J. Macromol. Sci., Rev. Macromol. Chem.* **C17** 297
Buchachenko A L, Kovarskii A L and Vasserman A M 1974 *Adv. Polym. Sci.* 26
[10] Bartoš J, Šauša O, Bandžuch P, Zrubcová J and Krištiak J 2002 *J. Non-Cryst. Solids* **307–310** 417
[11] Kilburn D, Wawryszczuk J, Dlubek G, Pionteck J, Hassler R and Alam M A 2006 *Macromol. Chem. Phys.* **207** 721
[12] Dlubek G, Shaikh M Q, Raetzke K, Paluch M and Faupel F 2010 *J. Phys.: Condens. Matter* **22** 235104
[13] Salgueiro W, Somoza A, Silva L, Consolati G, Quasso F, Mansilla M A and Marzocca A 2011 *Phys. Rev.* E **83** 051805
[14] Tao S 1972 *J. Chem. Phys.* **56** 5499
Eldrup M, Lightbody D and Sherwood J N 1981 *Chem. Phys.* **63** 51
Nakanishi N, Jean Y C, and Wang S J 1988 *Positron Annihilation Studies of Fluids* ed S CSharma (Singapore: World Scientific) p 292
[15] Böhmer R, Ngai K L and Angell C A 1993 *J. Chem. Phys.* **99** 201
[16] Bartoš J, Šauša O, J Krištiak J, Blochowicz T and E Rössler E 2001 *J. Phys.: Condens. Matter* **13** 11473
Bartoš J, Šauša O, Račko D, Krištiak J and Fontanella J J 2005 *J. Non-Cryst. Solids* **351** 2599
[17] Bartoš J, Majernik V, Iskrova M, Šauša O, Krištiak J, Lunkenheimer P and Loidl A 2010 *J. Non-Cryst. Solids* **356** 794
[18] Švajdlenková H, Šauša O, Ruff A, Lunkenheimer P, Loidl A and Bartoš J in preparation
[19] Bartoš J, Šauša O and Krištiak J 2004 Advanced Research Workshop (ARW) NATO Series *Nonlinear Dielectric Phenomena in Complex Liquids* (Dordrecht: Kluwer) p 289
[20] Bartoš J, Šauša O, Schwartz G A, Alegria A, Alberdi J M, Krištiak J and Colmenero J 2011 *J. Chem. Phys.* **134** 164507
Yu Y, Dlubek G, Bartoš J, Švajdlenková H and Krause-Rehberg R 2013 *Mat. Sci. Forum* **733** 179
Kilburn D, Wawryszczuk J, Dlubek G, Pionteck J, Hassler R and Alam M A 2006 *Macromol. Chem. Phys.* **207** 721
Bartoš J, Šauša O, Cangialosi D, Alegria A, Švajdlenkova H, Krištiak J, Arbe A and Colmenero J 2012 *J. Phys.: Condens. Matter* **24** 155104
Bartoš J, Schwartz G A, Šauša O, Alegria A, Krištiak J and Colmenero J 2010 *J. Non-Cryst. Solids* **356** 782
[21] Bartoš J, Šauša O, Köhler M, Švajdlenková H, Lunkenheimer P, Krištiak J and Loidl A 2011 *J. Non-Cryst. Solids* **357** 376
[22] Takahara S, Yamamuro Y and Suga H 1994 *J Non-Cryst. Solids* **171** 259
[23] Budil D E, Lee S, Saxena A S and Freed J H 1996 *J. Magn. Reson.* A **120** 155

[24] Krištiak J, Bartoš J, Krištiaková K and Bandžuch P 1994 *Phys. Rev.* B **49** 6601
[25] Kirkegaard P, Eldrup M, Mogensen O E and Pedersen N J 1989 *Comput. Phys. Commun.* **23** 307
[26] Thorpe T E and Rodger J W 1894 *Phil Trans Roy Soc London* **A185** 397
[27] Tamman G, and Hesse W 1926 *Z. Anorg. Allg. Chem.* **156** 245
[28] Mitsukuri S and Tonomura T 1927 and 1929 *Proc. Imper Academy of Japan* **3** 155 and **5** 23
[29] Denney D J 1959 *J. Chem. Phys.* **30** 159
[30] Ling A C and Willard J E 1968 *J. Phys. Chem.* **72** 1919
[31] Barlow A J, Lamb J and Matheson A J 1966 *Proc. R. Soc.* A **292** 322
[32] Schönhals A, Kremer F, Hofmann A, Fischer E W and Schlosser E 1993 *Phys. Rev. Lett.* **70** 3459
[33] Kivelson D, Kivelson S A, Zhao X L, Nussinov Z and Tarjus G 1995 *Physica* A **219** 27
[34] Sastry S 2000 *Phys. Chem. Commun.* **3** 79
[35] Schmidke B, Petzold N, Kahlau R, Hofmann M and Rössler E 2012 *Phys. Rev.* E **86** 041507
[36] Grest G S and Cohen M H 1980 *Phys. Rev.* B **28** 4113
Cohen M H and Grest G 1981 *Adv. Chem. Phys.* **48** 455
Paluch M, Casalini R and Roland C M 2003 *Phys. Rev.* E **67** 021508
[37] Ngai K L 1979 *Comm. Solid State Phys.* **9** 141
Ngai K L 2003 *J. Non-Cryst. Solids* **9** 1107
Casalini R, Ngai K L, Roland C M 2003 *Phys. Rev* E **68** 014201
[38] Kivelson D, Kivelson S A, Zhao X L, Nussinov Z and Tarjus G 1995 *Physica* A **219** 27
Kivelson D, Tarjus G, Zhao X L and Kivelson S A 1996 *Phys. Rev.* E **53** 751
Kivelson D and Tarjus G 1998 *J. Non-Cryst. Solids* **235–237** 86
[39] Eckstein E, Qian J, Hentschke R, Thurn-Albert T, Steffen W and Fischer E W 2000 *J. Chem. Phys.* **113** 4751
[40] Fischer E W and Sakai A 1999 Heterophase fluctuations in supercooled liquids and polymers *AIP Conf. Proc.* No. 469, ed M Tokuyama and I Oppenheim p 325
Fischer E W, Bakai A, Patkowski A, Steffen W and Reinhardt L 2002 *J. Non-Cryst. Solids* **307–310** 584
[41] Tanaka H 1998 *J Phys.: Condens. Matter* **10** L207
Tanaka H 1999 *J. Phys.: Condens. Matter* **11** L159
Tanaka H 1999 *J. Chem. Phys.* **111** 3163 and 3175
Tanaka T 2005 *J. Non-Cryst. Solids* **351** 3371, 3385 and 3396
[42] Hansen C, Stickel F, Berger T, Richert R and Fischer E W 1997 *J. Chem. Phys.* **107** 1086
[43] Kudlik A, Tschirwitz C, Benkhof S, Blochowicz T and Rössler E 1997 *Europhys. Lett.* **40** 649
[44] Sillrén P *et al* 2014 *J. Chem. Phys.* **140** 124501
[45] Pöschl M and Hertz H G 1994 *J. Chem. Phys.* **98** 8195
[46] Stickel F, Fischer E W and Richert R 1995 *J. Chem. Phys.* **102** 6251
[47] Richert R and Angell C A 1998 *J. Chem. Phys.* **108** 9016
[48] Wang L M, Angell C A and Richert R 2006 *J. Chem. Phys.* **125** 074505
[49] Winberg P, Eldrup M and Maurer F H J 2012 *J. Chem. Phys.* **136** 244902